

t -channel single-top production: the contribution of non-factorisable corrections

Christian Brønnum-Hansen,^a Jérémie Juvin-Quarroz,^a Chiara Signorile-Signorile^{a,b,c,*} and Chen-Yu Wang^c

^a*Institute for Theoretical Particle Physics, Karlsruhe Institute of Technology (KIT), Wolfgang-Gaede-Straße 1, 76131 Karlsruhe, Germany*

^b*Institute for Astroparticle Physics, Karlsruhe Institute of Technology (KIT), Hermann-von-Helmholtz-Platz 1, 76344 Eggenstein-Leopoldshafen, Germany*

^c*Max-Planck-Institut für Physik, Föhringer Ring 6, 80805 München, Germany*
E-mail: christian.broennum-hansen@kit.edu, jeremie.quarroz@kit.edu, chiara.signorile-signorile@kit.edu, cywang@mpp.mpg.de

In this document we summarise the results obtained for the non-factorisable corrections to t -channel single-top production [6–8] and discuss their relevance for 13 TeV and 100 TeV proton-proton collisions. As illustrative outcomes of our study, we present results for the total cross section and for selected observables relevant for proton-proton collisions at the LHC and the FCC.

TTP23-046, P3H-23-072

*The European Physical Society Conference on High Energy Physics (EPS-HEP2023)
21-25 August 2023
Hamburg, Germany*

*Speaker

1. Introduction

A significant portion of the top quarks generated at the LHC arises from electroweak interactions, specifically through the *t*-channel single-top production mechanism. Predictions for this process are fundamental, for example, in constraining the CKM matrix element V_{bt} , and in investigating potential anomalous couplings within the tWb vertex. QCD corrections to *t*-channel single-top production are well-understood up to the next-to-next-to-leading order (NNLO) under the so-called *factorisable approximation* [1–4], where interactions between different quark lines are disregarded (see the left panel of Fig.1 for an example of a Feynman diagram contributing to the factorisable corrections). Their impact is found to be relatively modest, affecting the cross section by only around 1%. Given the current state of theoretical precision, it becomes valuable to move beyond this approximation and calculate the *non-factorisable corrections* (see the right panel of Fig.1 for an example of Feynman diagram). Their contribution is null at NLO due to color conservation and is color-suppressed at NNLO by a factor of $N_c^2 - 1 = 8$ in comparison to the factorisable corrections. Nonetheless, recent arguments suggest that a π^2 enhancement factor, attributed to the Glauber phase, could potentially counterbalance this color suppression, as was explicitly demonstrated in the context of vector boson fusion within the eikonal approximation [5]. Such effect is peculiar of virtual corrections, and is related to the infinite perturbative interaction range between the two quark lines exchanging gluons. In principle, it does not require a scattering to occur. Indeed, virtual contributions are expected to be dominant in non-factorisable corrections.

In this document, we present a concise summary of the outcomes derived from the assessment of non-factorisable corrections to *t*-channel single-top production [6–8], and discuss their relative significance for proton-proton collisions at both 13 TeV and 100 TeV energies.

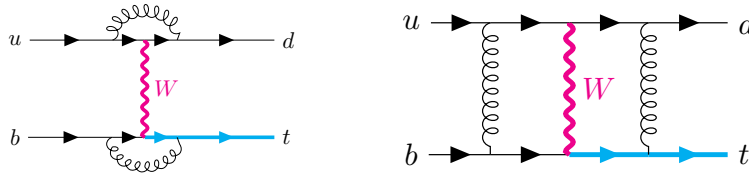


Figure 1: Example of Feynman diagram contributing to factorisable corrections (left panel) and to non-factorisable corrections (right panel). Massive top-quark is indicated with a blue solid line.

2. Ingredients of the calculation

The evaluation of non-factorisable corrections to *t*-channel single-top production requires the calculation of double-virtual, real-virtual and double-real corrections to the process $pp \rightarrow X + t$, where X is a quark of given flavour. In terms of the double-virtual correction, the primary challenge lies in computing the two-loop amplitude associated with non-factorisable diagrams, depicted in the right panel of Fig.1. This amplitude is determined numerically using the auxiliary mass flow method[9, 10]. For a more in-depth exploration, readers can refer to Ref. [6]. It is worth noting that we underscore the analytical reduction of the amplitude, preserving its complete dependence on the kinematic scales s , t , m_W , and m_t . The assessment of the pertinent master integrals demands only

a moderate amount of computational time. For a standard phase space point, achieving a precision of 20 digits takes approximately 30 minutes on a single core.

Next we consider the calculation of the real-virtual corrections. In this case, the main bottleneck is the evaluation of real-virtual amplitudes, due to the presence of numerous mass scales and to the necessity of having stable results also in kinematic regions where the radiation becomes unresolved. We note that working with anticommuting γ_5 in d dimensions, we can calculate form factors treating the weak current as a pure vector current, while fixing the external massless quarks to be left-handed. To treat the form factors we manage to express the real-virtual amplitude in terms of scalar box, triangle and bubble integrals. To improve the numerical stability of the amplitude, we switch to a basis of finite box integrals, restricting the divergent part to triangle integrals only, whose coefficients either become independent of the dimensional regulator ϵ or simply vanish.

The last component involves a tree-level, double-real correction, wherein two potentially unresolved gluons are emitted, linking both the massive and massless quark lines. To achieve fully detailed predictions, we utilise the nested soft-collinear subtraction scheme [11] to address the challenge of divergent phase-space integrals. In this specific process, only soft singularities can influence real-radiation amplitudes, and they are exclusively connected to independent emissions, resembling Abelian-like interactions. This observation significantly simplifies the subtraction procedure. While a minor complication arises from the presence of massive emitters, it does not compromise the analyticity of the method.

3. Phenomenology at the LHC and at the FCC

We consider proton-proton collisions at 13 TeV and at 100 TeV. We use the CT14 set for parton distribution functions (PDF) and the strong coupling constant. We match the perturbative order of the cross section to that of the PDF set, and use $m_t = 173.0$ GeV.

We first present the total cross section at a fixed factorisation scale $\mu_F = m_t$ at 13 TeV

$$\frac{\sigma_{pp \rightarrow X+t}}{1 \text{ pb}} = 117.96 + 0.26 \left(\frac{\alpha_s(\mu_R)}{0.108} \right)^2. \quad (1)$$

It is important to highlight that non-factorisable corrections emerge for the first time at NNLO, which makes determining an optimal choice for the renormalisation scale less straightforward. As seen in Eq. 1, altering the value of μ_R can lead to a notable modification in the impact of these corrections. For instance, with $\mu_R = m_t$, the non-factorisable corrections constitute approximately 0.2% of the LO cross section. In contrast, if we set μ_R to the typical transverse momentum of the top quark, $\mu_R = 40$ GeV, non-factorisable corrections rise to 0.35% of the LO cross section.

While seemingly small, non-factorisable corrections are quite comparable to the NNLO factorisable corrections to the NLO cross section. The latter were computed to be roughly -0.7% for similar choices of scales and parton distribution functions (refer to Table 7 in Ref.[4]). ¹

To delve deeper into the effects of various scale choices, Table 1 presents the relative impact of non-factorisable corrections with respect to the LO cross-section, for different values of the minimal top-quark transverse momentum ($p_{\perp}^{t,cut}$). We have set $\mu_F = m_t$ and allowed the renormalisation

¹The computations in Ref.[4] were conducted for proton-proton collisions at 14 TeV.

$p_{\perp}^{t,cut}$	$\sqrt{s} = 13 \text{ TeV}$		$\sqrt{s} = 100 \text{ TeV}$	
	$\mu_R = m_t$ $\delta_{\text{NNLO}} [\%]$	$\mu_R = 40 \text{ GeV}$ $\delta_{\text{NNLO}} [\%]$	$\mu_R = m_t$ $\delta_{\text{NNLO}} [\%]$	$\mu_R = 40 \text{ GeV}$ $\delta_{\text{NNLO}} [\%]$
0 GeV	0.22 ^{-0.04} _{+0.05}	0.34	0.16 ^{-0.03} _{+0.04}	0.25
20 GeV	0.23 ^{-0.04} _{+0.05}	0.36	0.17 ^{-0.03} _{+0.04}	0.26
40 GeV	0.25 ^{-0.04} _{+0.06}	0.39	0.19 ^{-0.03} _{+0.04}	0.29
60 GeV	0.26 ^{-0.04} _{+0.06}	0.41	0.20 ^{-0.03} _{+0.04}	0.32

Table 1: Dependence of the non-factorisable corrections on the transverse momentum of the top quark for different values of the renormalisation scale, at $\mu_F = m_t$. For each scale choice, we report the relative impact, δ_{NNLO} , of the non-factorisable contributions with respect to the LO cross section. Results for 13 TeV collisions are reported in the second and third columns, and for 100 TeV collisions in the fourth and fifth columns. See Refs. [7, 8] and the text for further details.

scale to vary. For $\mu_R = m_t$, we have also included scale variations corresponding to $\mu_R/2$ and $2\mu_R$. Notably, we observe that the non-factorisable contribution to the cross section increases by roughly $\mathcal{O}(8\%)$ as the p_{\perp}^t cut increases from 0 to 60 GeV, both for $\mu_R = m_t$ and $\mu_R = 40 \text{ GeV}$. In the same range the LO cross section decreases by $\mathcal{O}(11\%)$.

We now present the results for the integrated cross-section at 100 TeV

$$\frac{\sigma_{pp \rightarrow X+t}}{1 \text{ pb}} = 2367.0 + 3.8 \left(\frac{\alpha_s(\mu_R)}{0.108} \right)^2. \quad (2)$$

For a renormalisation scale $\mu_R = m_t$, the NNLO corrections amount to 0.16%, and increase to 0.25% for $\mu_R = 40 \text{ GeV}$. To compare the two energy regimes, 13 and 100 TeV, we conducted a similar analysis as described in the preceding paragraph. The results are summarised in Table 1, showcasing the impact of imposing different cuts on the top-quark transverse momentum while varying the renormalisation scale. It is noteworthy that at a center-of-mass energy of 100 TeV, the LO cross-section exhibits a relative decrease of approximately $\mathcal{O}(10\%)$ when setting $p_{\perp}^{t,cut} = 60 \text{ GeV}$. This trend closely parallels the one observed at 13 TeV. In contrast, non-factorisable corrections experience a slightly more pronounced increase compared to the 13 TeV result, with a change of $\mathcal{O}(13\%)$ for both $\mu_R = m_t$ and $\mu_R = 40 \text{ GeV}$.

We then consider differential distributions, and study the the impact of the non-factorisable corrections on the top-quark transverse momentum. In Fig. 2, the LO contribution is depicted with a solid blue line, while the non-factorisable corrections at $\mu \equiv \mu_F = \mu_R = m_t$ are shown with a dashed red line (the corresponding scale variation is indicated by the striped region). Additionally, the non-factorisable corrections at $\mu = 40 \text{ GeV}$ are represented by a green dashed line.

Upon examination of Fig.2, it becomes evident that both at $\sqrt{s} = 13 \text{ TeV}$ and $\sqrt{s} = 100 \text{ TeV}$, the non-factorisable corrections exhibit a dependence on p_{\perp}^t and share a similar shape. Notably, they are relatively small and negative at lower values of the transverse momentum. This pattern aligns with that of the double-virtual correction, as discussed in Ref.[6], an effect we anticipate to be kinematically favoured at lower p_{\perp}^t . In contrast, we observe a change in the sign of the corrections at

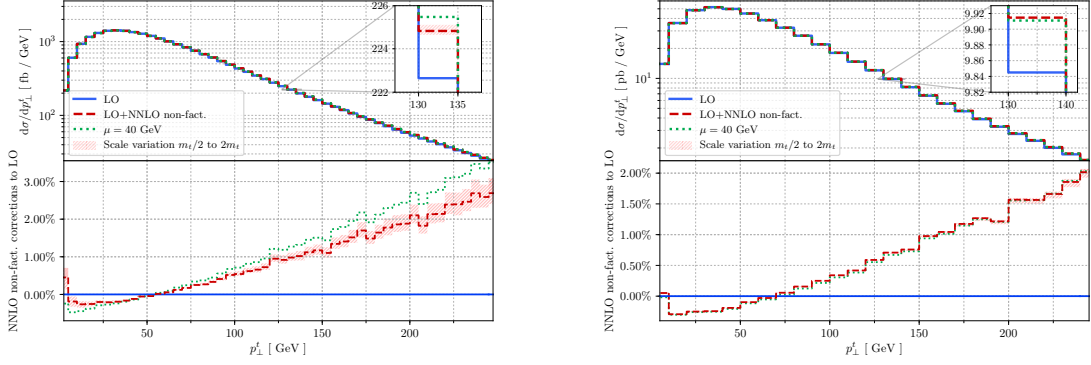


Figure 2: The transverse momentum distribution of the top quark is shown for two center-of-mass energies: $\sqrt{s} = 13$ TeV (left panel) and $\sqrt{s} = 100$ TeV (right panel). The blue solid line represents the Born cross section. The red dashed line corresponds to the non-factorisable corrections computed with $\mu \equiv \mu_F = \mu_R = m_t$. The striped region indicates the estimate of theoretical uncertainties via scale variation. Additionally, we include the p_{\perp}^t distribution at $\mu = 40$ GeV as a green dotted line.

different p_{\perp}^t values depending on the center-of-mass energy: occurring around 70 GeV for $\sqrt{s} = 100$ TeV and approximately 50 GeV for $\sqrt{s} = 13$ TeV.

We turn to the analysis of jet observables and focus on the transverse momentum distribution of the leading jet. To define jets we use the k_{\perp} -algorithm [12] and require them to have transverse momenta larger than 30 GeV and a radius of $R = 0.4$. From Fig. 3 we observe that the corrections to

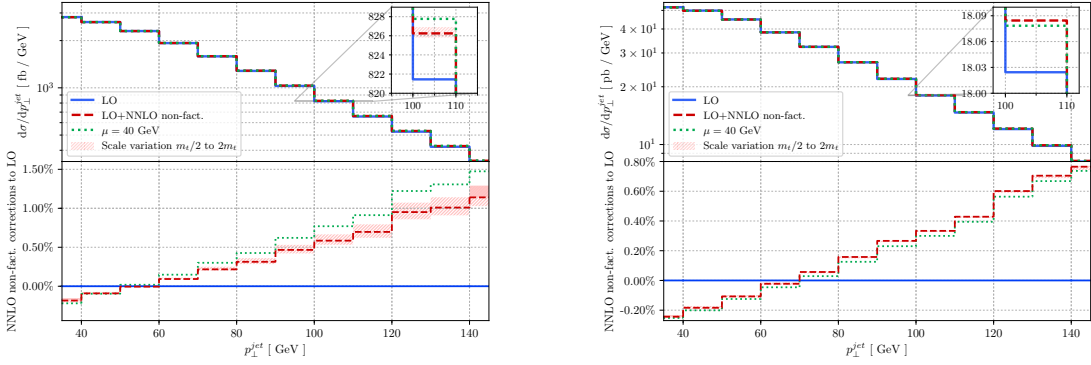


Figure 3: Leading jet transverse momentum distribution for $\sqrt{s} = 13$ TeV (left panel) and $\sqrt{s} = 100$ TeV (right panel). See the caption of Fig. 2 for details about the colours code.

the leading-jet transverse momentum are negative for p_{\perp}^{jet} smaller than ~ 50 GeV and reach about 1% at $p_{\perp}^{jet} \sim 140$ GeV for $\sqrt{s} = 13$ TeV. In contrast, at $\sqrt{s} = 100$ TeV the corrections change sign around 70 GeV and reach 0.7% at $p_{\perp}^{jet} \sim 140$ GeV.

4. Conclusions

This manuscript presents our recent calculation of *non-factorisable* corrections to the *t*-channel single-top production, which leads to the complete assessment of NNLO corrections for this process. We have outlined the impact of these non-factorisable corrections on both the total cross section and various kinematic distributions, considering proton-proton collisions at energies of 13 and 100 TeV. In the case of collisions at 13 TeV, we have demonstrated that non-factorisable contributions can be quite comparable to their factorisable counterparts in specific regions of the phase space. However, at 100 TeV, a direct comparison is currently unavailable due to the absence of results for the factorisable component. Such a comparison would be invaluable for gaining a deeper insight into the relative significance of these two categories of corrections, and it encourages similar analyses for different processes.

5. Acknowledgements

The authors thank Prof. Kirill Melnikov for contributing to the results quoted in this report. This research is partially supported by the Deutsche Forschungsgemeinschaft (DFG, German Research Foundation) under grant 396021762 - TTR 257. The work of C.B.H. presented here is supported by the Carlsberg Foundation, grant CF21-0486.

References

- [1] M. Brucherseifer, F. Caola and K. Melnikov, “On the NNLO QCD corrections to single-top production at the LHC”, *Phys. Lett. B* **736** (2014), 58-63
- [2] E. L. Berger, J. Gao, C. P. Yuan and H. X. Zhu, “NNLO QCD Corrections to t-channel Single Top-Quark Production and Decay”, *Phys. Rev. D* **94** (2016) no.7, 071501
- [3] E. L. Berger, J. Gao and H. X. Zhu, “Differential Distributions for t-channel Single Top-Quark Production and Decay at Next-to-Next-to-Leading Order in QCD”, *JHEP* **11** (2017), 158
- [4] J. Campbell, T. Neumann and Z. Sullivan, “Single-top-quark production in the *t*-channel at NNLO”, *JHEP* **02** (2021), 040
- [5] T. Liu, K. Melnikov and A. A. Penin, “Nonfactorizable QCD Effects in Higgs Boson Production via Vector Boson Fusion”, *Phys. Rev. Lett.* **123** (2019) no.12, 122002
- [6] C. Brønnum-Hansen, K. Melnikov, J. Quarroz and C. Y. Wang, “On non-factorisable contributions to t-channel single-top production”, *JHEP* **11** (2021), 130
- [7] C. Brønnum-Hansen, K. Melnikov, J. Quarroz, C. Signorile-Signorile and C. Y. Wang, “Non-factorisable contribution to t-channel single-top production”, *JHEP* **06** (2022), 061
- [8] C. Brønnum-Hansen, J. Quarroz, C. Signorile-Signorile and C. Y. Wang, “Non-factorisable contributions to *t*-channel single-top production at the LHC and FCC”, *PoS LL2022* (2022), 035

- [9] X. Liu, Y. Q. Ma and C. Y. Wang, “A Systematic and Efficient Method to Compute Multi-loop Master Integrals”, *Phys. Lett. B* **779** (2018), 353-357
- [10] X. Liu, Y. Q. Ma, W. Tao and P. Zhang, “Calculation of Feynman loop integration and phase-space integration via auxiliary mass flow”, *Chin. Phys. C* **45** (2021) no.1, 013115
- [11] F. Caola, K. Melnikov and R. Röntsch, “Nested soft-collinear subtractions in NNLO QCD computations”, *Eur. Phys. J. C* **77** (2017) no.4, 248
- [12] S. D. Ellis and D. E. Soper, “Successive combination jet algorithm for hadron collisions”, *Phys. Rev. D* **48** (1993), 3160-3166